








Prediction of a Heusler alloy with switchable metal-to-half-metal behavior

Vasily D. Buchelnikov ^{1,2} Vladimir V. Sokolovskiy ^{1,2} Olga N. Miroshkina ^{1,3,4} Danil R. Baigutlin ^{1,3}
Mikhail A. Zagrebin ^{1,2,5} Bernardo Barbiellini ^{3,6} and Erkki Lähderanta ³

¹*Faculty of Physics, Chelyabinsk State University, 454001 Chelyabinsk, Russia*

²*National University of Science and Technology "MISIS," 119049 Moscow, Russia*

³*Department of Physics, School of Engineering Science, LUT University, FI-53850 Lappeenranta, Finland*

⁴*Faculty of Physics and Center for Nanointegration Duisburg-Essen (CENIDE), University of Duisburg-Essen, 47048 Duisburg, Germany*

⁵*National Research South Ural State University, 454080 Chelyabinsk, Russia*

⁶*Physics Department, Northeastern University, Boston, Massachusetts 02115, USA*



(Received 13 November 2020; revised 29 December 2020; accepted 25 January 2021; published 8 February 2021)

We propose a ferromagnetic Heusler alloy that can switch between a metal and a half-metal. This effect can provide tunable spintronics properties. Using the density functional theory with reliable implementations of the electron correlation effects, we find Mn_2ScSi total energy curves consisting of distinct branches with a very small energy difference. The phase at low lattice crystal volume is a low magnetic half-metallic state while the phase at high lattice crystal volume is a high magnetic metallic state. We suggest that the transition between half-metallic and metallic states can be triggered by a triaxial contraction/expansion of the crystal lattice or by an external magnetic field if we assume that the lattice is cubic and remains cubic under expansion/contraction. However, the phase at high volume can also undergo an austenite-martensite phase transition because of the presence of Jahn-Teller active $3d$ electrons on the Mn atoms.

DOI: [10.1103/PhysRevB.103.054414](https://doi.org/10.1103/PhysRevB.103.054414)

I. INTRODUCTION

Nowadays, spintronics is a rapidly developing field of science and technology [1–4], which aims to use the intrinsic spin of the electron and its associated magnetic moment in solid-state devices [5,6], including synchronized networks of spin-transfer oscillators [7], spin-transfer torque [8] and magnetoelectric random access memory devices [9,10], spin transfer nanogenerators [11], and spin holographic processors [12]. The efficiency of these devices is related directly to the level of spin injection from the electrodes to the semiconductors and to their degree of spin polarization [13]. Half-metallic (HM) ferromagnetic (FM) compounds are characterized by an energy gap in one spin direction at the Fermi level. They therefore exhibit metallic character in one spin-channel and semiconducting behavior in the other spin-channel [14,15].

Among HM ferromagnets, the half- and full-Heusler alloys are of great interest because they usually demonstrate stable half-metallicity with high Curie temperature and spin polarization [14,16,17]. Nowadays much attention is given to the wide variety of FM Co_2YZ ($Y = \text{Fe, Mn}$ and $Z = \text{Si, Ge, Sn}$) [18–26], Fe_2YZ ($Y = \text{Cr, Mn, Co}$ and $Z = \text{Si, Al, Ga}$) [13,27–29], and ferrimagnetic (FIM) Mn_2YZ ($Y = \text{V, Cr, Fe, Co, Ni}$ and $Z = \text{Al, Ga, Si, Ge, Sn, In}$) [13,30–36] that were studied both theoretically and experimentally. In the Co_2YZ family, the HM behavior appears when the Y element has fewer valence electrons than Co. On the other hand, the half-metallicity in Fe_2YZ and Mn_2YZ families occurs regardless of the number of valence electrons in the Y atoms. Therefore, the HM behavior is promoted by the Mn and Fe atoms. Moreover,

parallel or antiparallel spin alignment of two Mn atoms can lead to FM and FIM order and to noncolinear configurations. Since the Mn^{3+} ion has a d^4 electronic configuration with partially filled e_g orbitals, it is Jahn-Teller active. This effect explains the tetragonal distortion producing high magnetocrystalline anisotropy (MCA). This observation makes FIM Mn_2 -based alloys useful for transfer torque application, where high MCA is a key factor for fast switching with low currents and high thermal stability [37,38].

An interesting idea to add Sc (with one d valence electron) into the matrix of the Mn_2 -based family was recently proposed by Ram *et al.* [13]. These authors performed density functional theory (DFT) calculations for Mn_2ScZ ($Z = \text{Si, Ge, Sn}$) Heusler alloys taking into account on-site Coulomb interaction effects. The results indicated HM behavior with a narrow band gap in the case of Mn_2ScSi and Mn_2ScGe whereas Mn_2ScSn displayed metallic behavior. Ram *et al.* [13] claimed that one must use an accurate DFT scheme to reproduce their results since the deficiencies of traditional DFT exchange correlation approximations such as the local spin density approximation (LSDA) and the generalized gradient approximation (GGA) prevent the appearance of HM properties in Mn_2ScZ alloys. Therefore, one must reduce the self interaction errors present in LSDA and GGA by using schemes such as the DFT + U method [39]. Recently, we studied the correlation effects beyond the GGA in α -Mn [40], Ni_2 -, and Co_2 -based Heusler alloys [25,41] by using the strongly constrained and appropriately normed (SCAN) functional [42] (meta-GGA method), which contains

self-interaction correction without introducing an explicit Hubbard parameter U .

In this work, we confirm that reliable corrections beyond the GGA not only stabilize the HM properties of the Mn_2ScSi alloys in a robust way, but reveal a surprisingly rich phase diagram useful for tunable spintronics applications. For example, one could produce spintronic logic devices with switches that can operate on femtosecond timescales [43]. Our results show that Mn_2ScSi is an exemplar magnetic functional material hosting competing phases. The lattice of this material provides an elastic environment where charge, spin, and orbital degrees of freedom interact and produce unexpected functionalities [44]. Small energy differences between phases also offer unique opportunities to benchmark Coulomb correlation effects in DFT.

The outline of the paper is as follows. Section II contains the calculation details. Section III is devoted to the discussion of the results of structural, magnetic, and electronic properties and phase stability of Mn_2ScSi . The concluding remarks are presented in Sec. IV.

II. CALCULATION DETAILS

To perform the calculations, we employed the projector augmented wave (PAW) method implemented in VASP code [45,46] using 16-atom supercells. The GGA for the exchange correlation functional was treated within the Perdew, Burke, and Ernzerhof (PBE) [47] scheme. Electron correlation effects beyond GGA were included using both GGA + U by Dudarev *et al.* [48] and meta-GGA SCAN by Sun *et al.* [42]. The parameter U for Mn is taken in the interval from 0.2 to 2 eV. The value $U_{\text{Mn}} = 1.973$ eV was chosen in accordance with Ram *et al.* [13]. Since the Coulomb correlation for Sc weakly affects the electronic and magnetic properties, we choose $U_{\text{Sc}} = 0.435$ eV, proposed by Ram *et al.* [13]. The volume optimization of regular and inverse Heusler structures (space groups $Fm\bar{3}m$ and $F\bar{4}3m$) with different magnetic order is performed. For all functionals, the geometry optimization procedure yields the regular L2₁-cubic Heusler structure as the most favorable one with the FIM order involving antiparallel alignment of Mn and Sc magnetic moments (see Supplemental Material (SM) [49]).

III. RESULTS AND DISCUSSIONS

A. Structural optimization

We first consider the total energy results. In Fig. 1, we show the total energy as a function of the lattice constant (a) and the total magnetic moment (μ_{tot}) calculated within SCAN and GGA + U . SCAN yields a degenerated ground state with two almost equal energy minima observed at lattice constants of 5.905 and 6.108 Å. These two minima correspond to two magnetic states with the values of μ_{tot} equal to 3 and 5.8 $\mu_B/\text{f.u.}$ as shown in Fig. 1(b). We denote these states as the low-magnetic state (LMS) and high-magnetic state (HMS), respectively. The energy and magnetic moment differences between LMS and HMS are $\Delta E = 3.75$ meV/atom and $\Delta\mu = 2.90$ $\mu_B/\text{f.u.}$, respectively. The total magnetic moment in SCAN is an integer in agreement with the empirical Slater-Pauling (SP) [50] rule, thereby revealing the HM behavior.

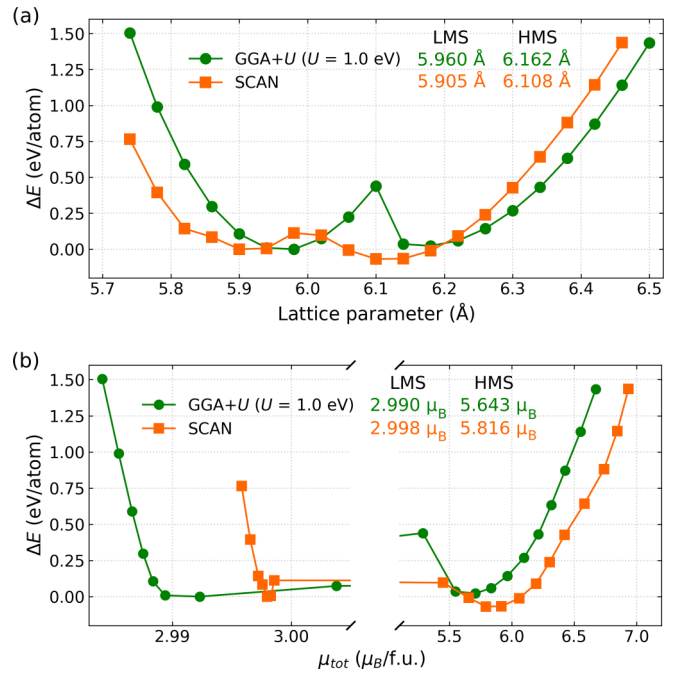


FIG. 1. The total energy difference (ΔE) as a function of (a) lattice parameter and (b) magnetic moment of Mn_2ScSi for SCAN and GGA + U ($U = 1$ eV) solutions. For each cases, the ΔE is plotted with respect to the left energy minimum.

In contrast to SCAN, our GGA calculations give only one clear minima at lattice constant $a_0 = 5.94$ Å. Ram *et al.* [13] only considered GGA + U corrections around the GGA total energy minima, but they missed the second total energy minima at higher volume. In our case, the volume optimization

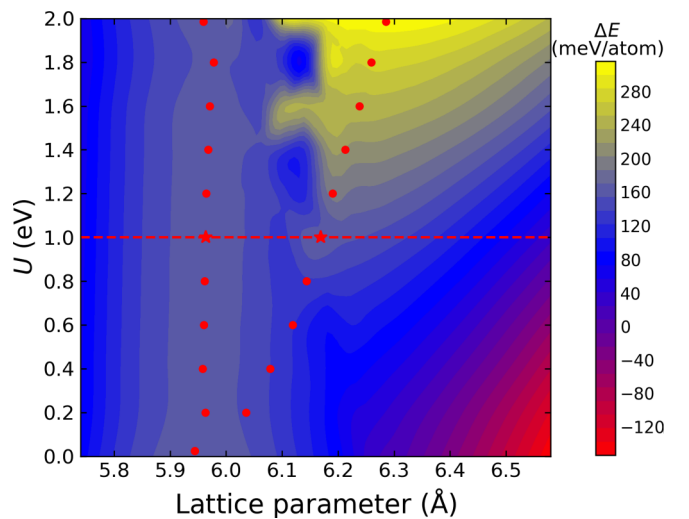


FIG. 2. The total energy difference for Mn_2ScSi calculated by GGA + U for a set of U values and mapped into the diagram “Coulomb repulsion term (U) – lattice parameter (a)”. ΔE is plotted with respect to the minimum for LMS. The optimized lattice parameters, which are estimated from the fitting for the Birch-Murnaghan equation of state for both LMS and HMS, are marked by the red symbols. The stars denote degeneracy of the ground state for which the LMS and HMS have a similar energy at $U = 1$ eV.

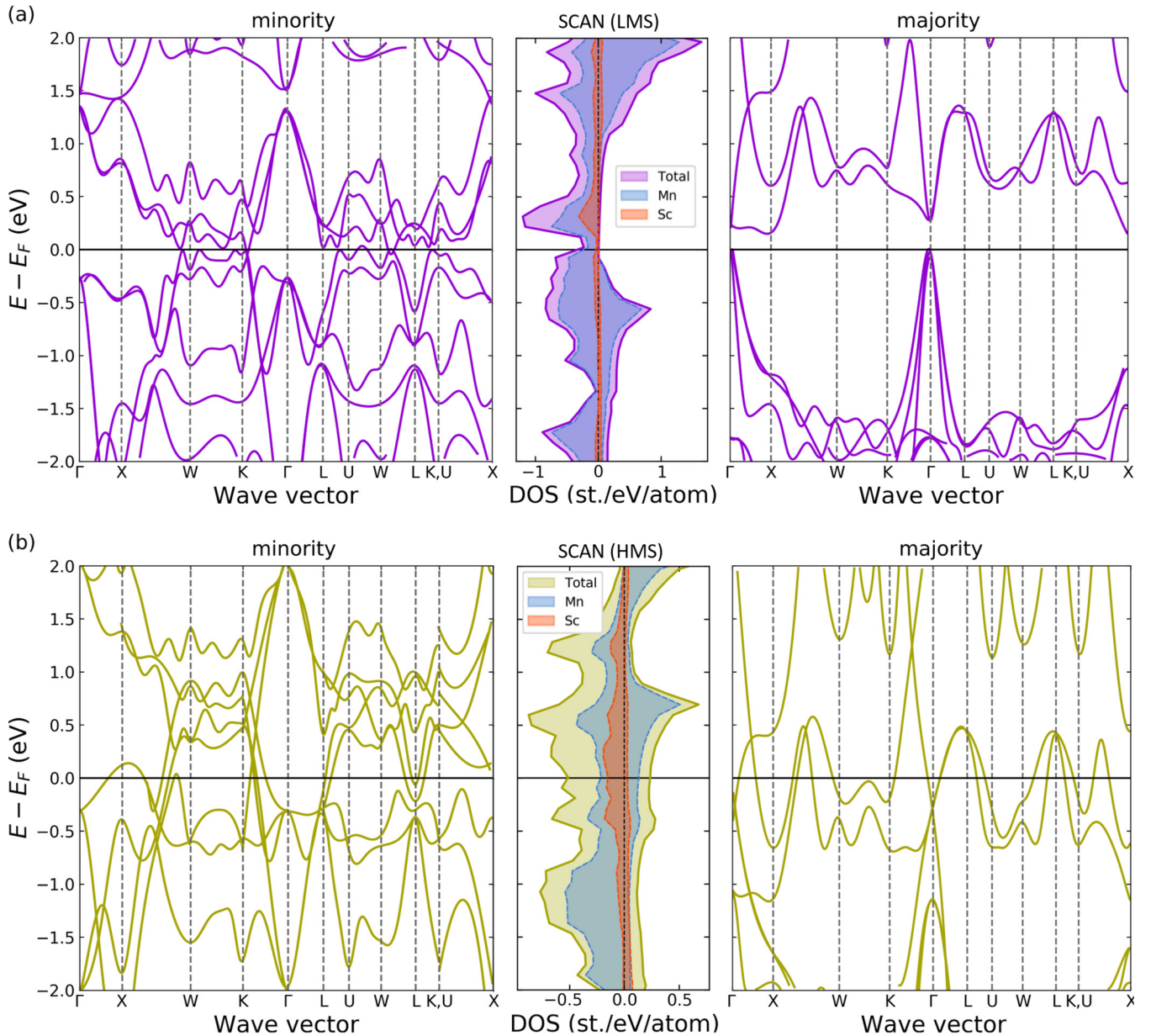


FIG. 3. SCAN energy band structure, total and partial DOSs of Mn_2ScSi calculated for the (a) LMS and (b) HMS with the optimized lattice constants $a_0^{\text{LMS}} = 5.905 \text{ \AA}$ and $a_0^{\text{HMS}} = 6.108 \text{ \AA}$, respectively.

with fixed U value of 1.973 eV as Ram *et al.* [13] yields both a local energy minimum at a similar equilibrium volume as GGA and the global minimum at larger volume as illustrated in the SM [49].

To better understand these results, we performed a parametric study of the Hubbard parameter U . Figure 2 illustrates a contour map of the total energy as functions of U and lattice parameter a . The set of $E(a)$ curves for various U is given in the SM [49]. We delineate in this contour map shown in Fig. 2 a triangle linking optimized lattice constants at local and global energy minima corresponding to the LMS and HMS, respectively. The vertex of this triangle is located close to U equal to zero, demonstrating that GGA is a singular point in terms of correlation effects. As soon as we introduce a small U value, two well-defined structures with different magnetization appear in the energy landscape. Related parametric

studies in γ -Mn by Podloucky and Redinger [51] and by Pulkkinen *et al.* [40] found that U at approximately 1 eV gives the corrected equilibrium volume. Therefore, we believe that $U \approx 1$ eV is a correct energy scale to describe the correlation effects in the present case. For $U = 1$ eV, the LMS and HMS are found to be close to each other in the energy as shown in Fig 1(a), in agreement with SCAN.

The transition between LMS and HMS can be achieved by a uniform contraction/expansion of the crystal lattice by $\approx 3.3\%$. We predict that the magnetovolume effect [52] ($\frac{\Delta V}{V_{\text{HMS}}}$) should be accompanied by the change in magnetization ($\Delta\mu_{\text{tot}}$) corresponding to $\approx 2.8 \mu_B/\text{f.u.}$ as it is derived from SCAN calculations. For GGA + U with $U = 1$ eV, $\Delta\mu_{\text{tot}}$ is slightly less and equals $\approx 2.7 \mu_B/\text{f.u.}$ Another way is to switch the transition by applying magnetic field.

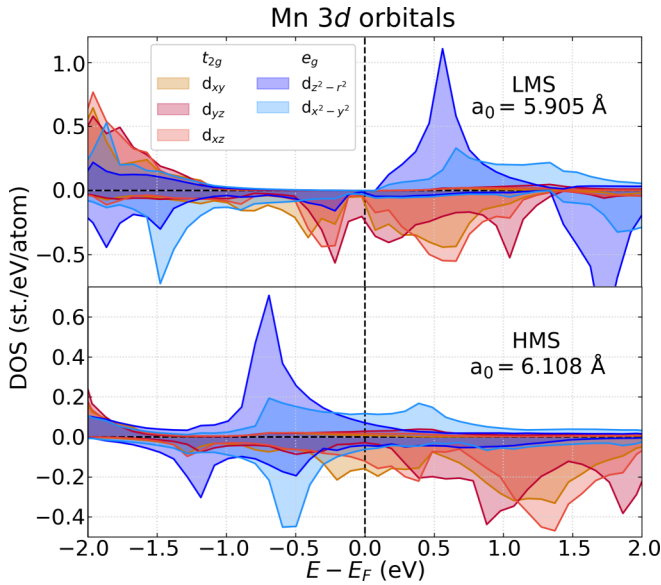


FIG. 4. Mn-3d orbital resolved DOSs for LMS (upper) and HMS (bottom) calculated with SCAN.

B. Electronic structure

To understand the electronic structure, we consider the spin-polarized band structures and the density of states (DOS). The bands are calculated along the high-symmetric points of the first Brillouin zone for the majority and minority spin channels for the GGA, GGA + U , and SCAN methods. In Fig. 3, we present both the SCAN bands and DOS curves calculated at the optimized lattice constants for LMS and HMS found in Fig. 1(a). The corresponding figures for GGA and GGA + U are given in the SM [49]. As Fig. 3(a) suggests, in the case of LMS, the minority-spin bands present few band crossings at the Fermi level (E_F), while the majority-spin bands reveal a clear energy gap around E_F . Such HM behavior for Mn_2ScSi is quite different of that in regular HM Heusler alloys in which the spin up states are filled and the spin down states are unoccupied at E_F [37]. The energy gap at Γ point for the majority bands is direct as shown in Fig. 3(a) and its predicted value within SCAN is 0.32 eV which is twice the value calculated by Ram *et al.* [13].

In terms of the HMS [Fig. 3(b)], both the minority and majority spin bands as well as DOSs show clear metallic behavior. It is important to notice that the bands calculated for the GGA + U with $U = 1.973$ eV at the optimized volume [49] display metallic character, in contrast to the bands reported by Ram *et al.* [13], indicating that the HM properties are lost for the larger volume. Therefore, it is possible to switch the HM behavior by a uniform contraction/expansion of the crystal lattice.

Such switching behavior can be rationalized by analyzing the 3d partial DOSs for Mn atoms in the vicinity of E_F shown in Fig. 4. For the LMS, three t_{2g} orbitals at E_F are present in the minority spin channel and contribute to the integer magnetic moment, whereas two e_g orbitals are almost empty. In contrast, both the t_{2g} and e_g orbitals at E_F for the minority spin channel are occupied for the HMS. For the majority spin channel we observe mostly e_g orbitals. The main difference

between LMS and HMS is the occupation of an energy e_g peak for the majority spin band. When the e_g state is occupied the system undergoes an austenitic-martensite transition because of Jahn-Teller effects.

Our results above apply if the lattice is cubic and remains cubic under triaxial expansion/contraction [53]. To examine the martensitic phase, we performed total energy calculations as a function of tetragonal distortion ratio c/a assuming a constant volume between austenite ($c/a = 1$) and martensite ($c/a \neq 1$). Indeed the martensitic phase with $c/a = 1.27$ is found to be energetically favorable [49]. The predicted $\Delta\mu_{\text{tot}}$ between the austenitic and martensitic phases is about $1.807 \mu_B/\text{f.u.}$ This finding allows us to conclude that Mn_2ScSi should also display magnetocaloric properties in the vicinity of magnetostuctural phase transformation [54].

C. Phase stability

Since the predicted Mn_2ScSi compound has not yet been grown, it is important to evaluate its phase stability. We therefore checked the thermodynamic stability in three steps.

As a preliminary test, we performed formation energy (E_{form}) calculations for Mn_2ScSi with respect to the elemental components in their ground-state bulk structures. The negative values of $E_{\text{form}}^{\text{SCAN}}$ (-0.312 and -0.319 eV/atom for LMS and HMS, respectively) indicate the thermodynamic stability of Mn_2ScSi in the corresponding cubic states [49].

However, stability with respect to the sum of total energies of the corresponding pure elements is a necessary but not yet a sufficient condition for thermodynamic phase stability. To clarify this point, we must compare also the E_{form} of a compound against all stable combination of phases at that composition. This aim can be achieved with the convex hull construction for the phase space of interest [55]. Typically, a convex hull connects stable phases that are lower in E_{form} than any other phase under consideration in this overall composition. In this way, the phases located above the convex hull are metastable or unstable while phases placed on the convex hull are stable. The pivot points (12 stable phases) for the convex hull of the Mn-Sc-Si ternary system were taken according to the AFLOW database [55] (they are listed in Table II of the SM [49]). By considering the $E_{\text{form}}^{\text{SCAN}}$ of these phases, we constructed the three-dimensional convex hull shown in Fig. 5(a). Here, we indicate $E_{\text{form}}^{\text{SCAN}}$ for Mn_2ScSi with the LMS cubic structure and HMS tetragonal one. The formation energies of pure elements are set to zero. We show the cross section of the hull energy convex in Fig. 5(b) to estimate the distance from the most stable phase. The Mn_2ScSi is located above the convex hull by ≈ 0.24 eV/atom for the LMS cubic phase as shown in Fig. 5(b). Interestingly, this distance is about 0.188 eV/atom [55] for GGA-PBE. Thereby, this result suggests a metastable tendency of the Mn_2ScSi compound.

To understand this metastable behavior, we compare the Mn_2ScSi phase energy to the energies of decomposition products (pivot points of the convex hull) at that composition and calculate the mixing energy E_{mix} . To accomplish this task, we consider 23 possible decomposition reactions into the three stable components (see Table III and Fig. 7 in the SM [49]). As a result, we found that 9 of 23 reactions yield a negative sign E_{mix} indicating the stability of the LMS cubic phase against

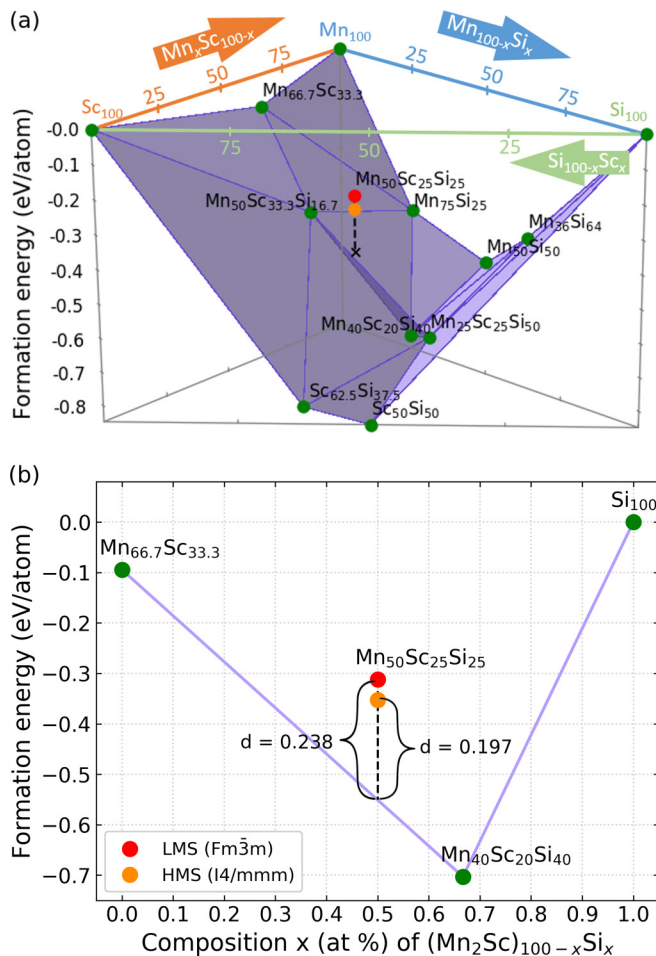


FIG. 5. (a) The hull energy convex and (b) cross section of hull energy convex that contains the convex hull distance for Mn_2ScSi with the LMS cubic structure and HMS tetragonal one. The formation energies are calculated with SCAN.

to segregation process. Therefore, we conclude that Mn_2ScSi can be grown as a metastable compound. We must keep in mind that the well-known $Ni_2Mn_{1+x}Z_{1-x}$ Heusler alloys show both experimentally and theoretically a segregation tendency into ternary stoichiometric and binary compounds [56–59] due to several-step heat treatment. Despite this metastable character, Ni_2Mn -based alloys still exhibit remarkable multifunctional properties.

IV. CONCLUSION

In conclusion, accurate DFT calculations in Mn_2ScSi Heusler alloy reveal an almost equal double energy minima

behavior for close lattice constants but different magnetic moments. Mn_2ScSi displays either half-metallic (in LMS) or metallic (in HMS) behavior as a function of the lattice parameter. Our study shows how one can preserve the HM phase or one can switch to the metallic phase. We suggest that the half-metallic \leftrightarrow metallic transition might be realized by applying an external magnetic field or pressure. The critical magnetic field evaluated from the relation between ΔE and Zeeman energy is about 11 T. While the magnetovolume effect and critical pressure are predicted to be 3.3% and 20 GPa, respectively. A second interesting aspect of the correlation effects is related to the prediction of an austenite-martensite transformation for the metallic phase, which produces a change in magnetization and a magnetocaloric effect.

We suggest that the switching mechanism between half-metallic and metallic behavior could be implemented for the design of spintronics devices like spin filters, sensors, switches, logical gates with femtosecond timescale [43]. Till date many studies were performed theoretically and experimentally to investigate the externally controlled carrier’s spin polarization and half-metallic–metallic transition in HM Heusler alloys by applying pressure, magnetic, or electric fields [25,60–62]. However, in all these cases, the external load was applied for a certain length of time, which implies significant energy consumption. In the present work, the proposed switching behavior in Mn_2ScSi can be realized at once. Since this external perturbation is limited in time, the energy consumption is significantly lowered. This finding opens new avenues for fast and energy efficient spintronics applications.

ACKNOWLEDGMENTS

SCAN calculations were supported by the Russian Science Foundation (RSF) Project No. 17-72-20022. GGA calculations were performed with the support of the Ministry of Science and Higher Education of the Russian Federation within the framework of the Russian State Assignment under Contract No. 075-00250-20-03. GGA + U calculations were funded by the Russian Foundation for Basic Research (RFBR) Grant No. 20-42-740006. B.B. acknowledges CSC-IT Center for Science, Finland, for computational resources and support from the COST Action CA16218. O.N.M. acknowledges the Deutsche Forschungsgemeinschaft (DFG, German Research Foundation) Project-ID 405553726: TRR 270, subproject B06. V.D.B. and M.A.Z. gratefully acknowledge the financial support of the Ministry of Science and Higher Education of the Russian Federation in the framework of Increase Competitiveness Program of NUST “MISIS” (No. K2-2020-018), implemented by a governmental decree, No. 211.

[1] W. Gallagher, *Emerging Spintronic Memories* (CRC Press, Boca Raton, FL, 2019), pp. 443–470.
 [2] A. Fert, *Rev. Mod. Phys.* **80**, 1517 (2008).
 [3] B. Dieny, I. L. Prejbeanu, K. Garello, P. Gambardella, P. Freitas, R. Lehndorff, W. Raberg, U. Ebels, S. O. Demokritov, J. Akerman, A. Deac, P. Pirro, C. Adelman, A. Anane,

A. V. Chumak, A. Hirohata, S. Mangin, Sergio O. Valenzuela, M. Cengiz Onbaşlı, M. d’Aquino, G. Prenat, G. Finocchio, L. Lopez-Diaz, R. Chantrell, O. Chubykalo-Fesenko, and P. Bortolotti, *Nature Electronics* **3**, 446 (2020).
 [4] J. Puebla, J. Kim, K. Kondou, and Y. Otani, *Communications Materials* **1**, 24 (2020).

- [5] S. Bhatti, R. Sbiaa, A. Hirohata, H. Ohno, S. Fukami, and S. Piramanayagam, *Mater. Today* **20**, 530 (2017).
- [6] A. Hirohata, K. Yamada, Y. Nakatani, I.-L. Prejbeanu, B. Diény, P. Pirro, and B. Hillebrands, *J. Magn. Magn. Mater.* **509**, 166711 (2020).
- [7] J. Torrejon, M. Riou, F. A. Araujo, S. Tsunegi, G. Khalsa, D. Querlioz, P. Bortolotti, V. Cros, K. Yakushiji, A. Fukushima, H. Kubota, S. Yuasa, M. D. Stiles, and J. Grollier, *Nature* **547**, 428 (2017).
- [8] Y.-C. Liao, C. Pan, and A. Naeemi, *IEEE J. Explor. Solid-State Computat.* **6**, 9 (2020).
- [9] H. Zhang, W. Kang, K. Cao, B. Wu, Y. Zhang, and W. Zhao, *IEEE Trans. Electron Devices* **66**, 2017 (2019).
- [10] T. Wu, A. Bur, K. Wong, P. Zhao, C. S. Lynch, P. K. Amiri, K. L. Wang, and G. P. Carman, *Appl. Phys. Lett.* **98**, 262504 (2011).
- [11] L. Fu, Z. Cao, S. Hemour, K. Wu, D. Houssameddine, W. Lu, S. Pistorius, Y. Gui, and C.-M. Hu, *Appl. Phys. Lett.* **101**, 232406 (2012).
- [12] Y. K. Fetisov and A. S. Sigov, *RENSIT* **10**, 343 (2018).
- [13] M. Ram, A. Saxena, A. E. Aly, and A. Shankar, *RSC Adv.* **10**, 7661 (2020).
- [14] L. Bainsla and K. Suresh, *Appl. Phys. Rev.* **3**, 031101 (2016).
- [15] M. Shakil, H. Arshad, M. Zafar, M. Rizwan, S. S. A. Gillani, and S. Ahmed, *Mol. Phys.* **118**, e1789770 (2020).
- [16] C. Palmström, *MRS Bull.* **28**, 725 (2003).
- [17] H. Mori, Y. Odahara, D. Shigyo, T. Yoshitake, and E. Miyoshi, *Thin Solid Films* **520**, 4979 (2012).
- [18] D. Hoat, J. Rivas-Silva, and A. M. Blas, *J. Comput. Electron.* **17**, 1470 (2018).
- [19] B. Deka, D. Chakraborty, and A. Srinivasan, *Physica B* **448**, 173 (2014).
- [20] L. Siakeng, G. M. Mikhailov, and D. Rai, *J. Mater. Chem. C* **6**, 10341 (2018).
- [21] R. Y. Umetsu, A. Okubo, and R. Kainuma, *J. Appl. Phys.* **111**, 073909 (2012).
- [22] D. Comtesse, B. Geisler, P. Entel, P. Kratzer, and L. Szunyogh, *Phys. Rev. B* **89**, 094410 (2014).
- [23] M. A. Zagrebin, V. V. Sokolovskiy, and V. D. Buchelnikov, *J. Phys. D Appl. Phys.* **49**, 355004 (2016).
- [24] M. Meinert, C. Friedrich, G. Reiss, and S. Blügel, *Phys. Rev. B* **86**, 245115 (2012).
- [25] O. N. Miroshkina, D. R. Baigutlin, V. V. Sokolovskiy, M. A. Zagrebin, A. Pulkkinen, B. Barbiellini, E. Lähderanta, and V. D. Buchelnikov, *J. Appl. Phys.* **127**, 175108 (2020).
- [26] I. Galanakis, K. Özdoğan, B. Aktaş, and E. Şaşıoğlu, *Appl. Phys. Lett.* **89**, 042502 (2006).
- [27] S. Chaudhuri, V. Srihari, A. Nigam, and P. Bhoje, *J. Appl. Phys.* **126**, 083904 (2019).
- [28] S. He, Y. Liu, Y. Zheng, Q. Qin, Z. Wen, Q. Wu, Y. Yang, Y. Wang, Y. P. Feng, K. L. Teo, and C. Panagopoulos, *Phys. Rev. Materials* **1**, 064401 (2017).
- [29] L. Hongzhi, Z. Zhiyong, M. Li, X. Shifeng, L. Heyan, Q. Jingping, L. Yangxian, and W. Guangheng, *J. Phys. D* **40**, 7121 (2007).
- [30] H. Luo, Z. Zhu, G. Liu, S. Xu, G. Wu, H. Liu, J. Qu, and Y. Li, *J. Magn. Magn. Mater.* **320**, 421 (2008).
- [31] H. Zenasni, H. Faraoun, and C. Esling, *J. Magn. Magn. Mater.* **333**, 162 (2013).
- [32] H. Luo, H. Zhang, Z. Zhu, L. Ma, S. Xu, G. Wu, X. Zhu, C. Jiang, and H. Xu, *J. Appl. Phys.* **103**, 083908 (2008).
- [33] V. V. Sokolovskiy, M. A. Zagrebin, Y. Sokolovskaya, and V. D. Buchelnikov, *Solid State Phenom.* **233-234**, 229 (2015).
- [34] S. Chadov, X. Qi, J. Kübler, G. H. Fecher, C. Felser, and S. C. Zhang, *Nat. Mater.* **9**, 541 (2010).
- [35] T. Graf, S. S. P. Parkin, and C. Felser, *IEEE Trans. Magn.* **47**, 367 (2010).
- [36] A. K. Nayak, M. Nicklas, S. Chadov, P. Khuntia, C. Shekhar, A. Kalache, M. Baenitz, Y. Skourski, V. K. Guduru, A. Puri, U. Zeitler, J. M. D. Coey, and C. Felser, *Nat. Mater.* **14**, 679 (2015).
- [37] C. Felser, L. Wollmann, S. Chadov, G. H. Fecher, and S. S. P. Parkin, *APL Mater.* **3**, 041518 (2015).
- [38] J. Winterlik, S. Chadov, A. Gupta, V. Alijani, T. Gasi, K. Filsinger, B. Balke, G. H. Fecher, C. A. Jenkins, F. Casper, J. Kübler, G.-D. Liu, L. Gao, S. S. P. Parkin, and C. Felser, *Adv. Mater.* **24**, 6283 (2012).
- [39] M. Cococcioni and S. de Gironcoli, *Phys. Rev. B* **71**, 035105 (2005).
- [40] A. Pulkkinen, B. Barbiellini, J. Nokelainen, V. Sokolovskiy, D. Baigutlin, O. Miroshkina, M. Zagrebin, V. Buchelnikov, C. Lane, R. S. Markiewicz, A. Bansil, J. Sun, K. Pussi, and E. Lähderanta, *Phys. Rev. B* **101**, 075115 (2020).
- [41] V. D. Buchelnikov, V. V. Sokolovskiy, O. N. Miroshkina, M. A. Zagrebin, J. Nokelainen, A. Pulkkinen, B. Barbiellini, and E. Lähderanta, *Phys. Rev. B* **99**, 014426 (2019).
- [42] J. Sun, A. Ruzsinszky, and J. P. Perdew, *Phys. Rev. Lett.* **115**, 036402 (2015).
- [43] P. Tengdin, C. Gentry, A. Blonsky, D. Zusin, M. Gerrity, L. Hellbrück, M. Hofherr, J. Shaw, Y. Kvashnin, E. K. Delczeg-Czirjak, M. Arora, H. Nembach, T. J. Silva, S. Mathias, M. Aeschlimann, H. C. Kapteyn, D. Thonig, K. Koumpouras, O. Eriksson, and M. M. Murnane, *Sci. Adv.* **6**, eaaz1100 (2020).
- [44] T. Kakeshita, T. Fukuda, A. Saxena, and A. Planes, *Disorder and Strain-Induced Complexity in Functional Materials*, Vol. 148 (Springer, New York, 2011).
- [45] G. Kresse and J. Furthmüller, *Phys. Rev. B* **54**, 11169 (1996).
- [46] G. Kresse and D. Joubert, *Phys. Rev. B* **59**, 1758 (1999).
- [47] J. P. Perdew, K. Burke, and M. Ernzerhof, *Phys. Rev. Lett.* **77**, 3865 (1996).
- [48] S. L. Dudarev, G. A. Botton, S. Y. Savrasov, C. J. Humphreys, and A. P. Sutton, *Phys. Rev. B* **57**, 1505 (1998).
- [49] See Supplemental Materials at <http://link.aps.org/supplemental/10.1103/PhysRevB.103.054414> for additional information about the calculation details and the results of *ab initio* ground-state calculations for Mn₂ScSi.
- [50] According to the SP rule for HM systems, the total magnetic moment is equal to $\mu_{\text{tot}} = N_e - 24$, where N_e is the total number of valence electrons. For Mn₂ScSi, N_e is 21, and so $\mu_{\text{tot}} = 3\mu_B$. f.u. by absolute value is expected. Notice that the negative sign of μ_{tot} yields the energy gap at the Fermi level for the majority of the density of states.
- [51] R. Podloucky and J. Redinger, *J. Phys. Condens. Matter* **31**, 054001 (2018).
- [52] $\frac{\Delta V}{V_{\text{HMS}}} = \frac{V_{\text{HMS}} - V_{\text{LMS}}}{V_{\text{HMS}}}$, here V_{HMS} and V_{LMS} are the volume cells of HMS and LMS, respectively.
- [53] We checked the stability of LMS and HMS in a cubic phase to verify that the solution converges to the cubic lattice by

- considering a full structural relaxation using supercells with artificially broken symmetries. Our calculations showed that the cubic symmetry is preserved for both LMS and HMS if the relaxation calculations were performed in the vicinity of corresponding optimized lattice constants a_0 .
- [54] A. Planes, L. Mañosa, and M. Acet, *J. Phys. Condens. Matter* **21**, 233201 (2009).
- [55] C. Oses, E. Gossett, D. Hicks, F. Rose, M. J. Mehl, E. Perim, I. Takeuchi, S. Sanvito, M. Scheffler, Y. Lederer, O. Levy, C. Toher, and S. Curtarolo, *J. Chem. Inf. Model.* **58**, 2477 (2018); also see <http://www.aflowlib.org>.
- [56] W. Yuhasz, D. Schlage, Q. Xing, R. McCallum, and T. Lograsso, *J. Alloys Compd.* **492**, 681 (2010).
- [57] A. Çakır, M. Acet, U. Wiedwald, T. Krenke, and M. Farle, *Acta Mater.* **127**, 117 (2017).
- [58] T. Krenke, A. Çakır, F. Scheibel, M. Acet, and M. Farle, *J. Appl. Phys.* **120**, 243904 (2016).
- [59] V. V. Sokolovskiy, M. E. Gruner, P. Entel, M. Acet, A. Çakır, D. R. Baigutlin, and V. D. Buchelnikov, *Phys. Rev. Materials* **3**, 084413 (2019).
- [60] M. Zayed, A. Elabbar, and O. Yassin, *J. Alloys Compd.* **737**, 790 (2018).
- [61] J. Zhou, B. Sa, Z. Sun, C. Si, and R. Ahuja, *RSC Adv.* **5**, 73814 (2015).
- [62] J. Zhang, X. Li, and J. Yang, *J. Mater. Chem. C* **3**, 2563 (2015).